Electron-electron correlation in two-photon double ionization of He-like ions

S. X. Hu (胡素兴)

Electron-electron Correlation in Two-Photon Double Ionization of He-Like Ions

S. X. Hu (**胡素兴**)[*]

*E-mail:shu@lle.rochester.edu

Laboratory for Laser Energetics, University of Rochester,

250 E. River Road, Rochester, NY 14623

ABSTRACT

Electron correlation plays a crucial role in quantum many-body physics ranging from molecular bonding, strong-field–induced multi-electron ionization, to superconducting in materials. Understanding the dynamic electron correlation in the photoionization of relatively simple quantum three-body systems, such as He and He-like ions, is an important step toward manipulating complex systems through photo-induced processes. Here we have performed *ab initio* investigations of two-photon double ionization (TPDI) of He and He-like ions [Li^+, Be^{2+}, and C^{4+}] exposed to intense attosecond x-ray pulses. Results from such fully correlated quantum calculations show weaker and weaker electron correlation effects in TPDI spectra as the ionic charge increases, which is opposite to the intuition that the absolute increase of correlation in ground state should lead to more equal-energy sharing in photoionization. These findings indicate that the final-state electron–electron correlation ultimately determines their energy sharing in TPDI.

PACS numbers: 32.80.Fb, 32.80.Rm, 42.65. Re

I. INTRODUCTION

Electron-electron correlation plays a key role in understanding a variety of many-body phenomena in modern physics [1,2] and chemistry [3], ranging from superconductivity, molecular bonding, high-harmonic generation in multi-electron systems [4], and their ionization dynamics in intense few-cycle laser pulses [5]. Just like the essential role of electron exchange-correlation (xc) functional to density-functional theory [6] for quantum many-body systems, the electron–electron correlation in quantum few-body systems holds the key to unraveling its fundamental effects on a wide range of phenomena in atomic and molecular physics [7]. For the simplest quantum few-body systems such as He or He-like ions, significant theoretical and experimental advances have been made in recent years. On the theory side, the fully correlated motion of two indistinguishable electrons can now be understood by numerically solving the six-dimensional (6-D) Schrödinger equation, with methods like convergent close coupling [8], time-dependent close coupling [9], exterior complex scaling [10], and the R-matrix method [11]. In experiments, the rich dynamics of such three-body breakup processes can also be mapped out by advanced techniques like COLTRIMS (cold target recoil ion momentum spectroscopy) [12].

Extensive studies on electron correlation in photoionization of He have been carried out in past two decades [13–20]. However, the correlation effects in He-like ions have only been studied to date for single-photon double ionizations [21-23]. It is expected that as the nuclear charge increases, the two electrons in a deeper Coulomb potential will become even more strongly correlated. This is witnessed by the increasing xc-energy between the two electrons in their ground state of He-like ions, with respect to the independent-electron model. Namely, the

absolute repulsion energy ($1/r_{12}$) increases in He-like ions as Z increasing, even though its relative ratio to the total energy may become smaller. In addition, the two outgoing electrons will be even more affected by the strong Coulomb field [24,25] of He-like ions. Therefore, one would expect that the two photo-ionized electrons should be more strongly correlated (thereby sharing their energies more equally) in He-like ions than the He case. This belief is based on observations in which initial-state correlation is important in the photoionization of He [26–31].

In this paper, we have performed *ab initio* studies on two-photon double ionization (TPDI) of He and He-like ions of Li^+, Be^{2+}, and C^{4+} exposed to intense and ultrashort x-ray pulses. We choose the x-ray photon energy above the single-photon double-ionization (SPDI) threshold so that sequential TPDI is possible (i.e., each electron absorbs a single photon independently). By looking at how the resulting two electron spectra differ from the independent sequential TPDI (STPDI) picture, we can characterize the electron correlation effect. If the increase of absolute correlation energy dominates electron-electron energy sharing, one should expect the C^{4+} case will deviate much more from the STPDI picture than the He case. On the contrary, our results show the opposite.

The paper is arranged as follows: we shall briefly give the calculation method in Sec. II, which is followed by discussion of results in Sec. III. The conclusion is drawn in Sec. IV.

II.   THE TIME-DEPENDENT CLOSE-COUPLING METHOD

Our *ab initio* investigations on the electron correlation in TPDI of He and He-like ions are carried out by numerically solving the 6-D time-dependent Schrödinger equation (TDSE). We consider fully correlated, two-active-electron He, Li^+, Be^{2+}, and C^{4+} interacting with an

intense, linearly polarized ultrashort x-ray pulse. The fully correlated two-electron motion is governed by the 6-D TDSE of the following form (atomic units are used throughout):

$$i\frac{\partial}{\partial t}\phi\left(\mathbf{r}_1,\mathbf{r}_2\,|t\right)=$$

$$\left[-\frac{1}{2}\left(\nabla_1^2+\nabla_2^2\right)-\frac{Z}{r_1}-\frac{Z}{r_2}+\frac{1}{\left|\mathbf{r}_1-\mathbf{r}_2\right|}+\mathbf{E}_x\left(t\right)\square\left(\mathbf{r}_1+\mathbf{r}_2\right)\right]\phi\left(\mathbf{r}_1,\mathbf{r}_2\,|t\right),$$

(1)

where $\mathbf{r}_1$ and $\mathbf{r}_2$ are the position vectors of each electron, with respect to the nucleus having a charge Z. The x-ray pulse $[E_x(t)]$ interacts with both electrons in the dipolar form. A more-tractable solution can be obtained by following the time-dependent close-coupling (TDCC) recipe [32]: expanding the 6-D wave function $\phi(\mathbf{r}_1,\mathbf{r}_2|t)$ in terms of bipolar spherical harmonics

$$Y_{l_1l_2}^{L,M}\left(\Omega_1,\Omega_2\right),\Phi\left(\mathbf{r}_1,\mathbf{r}_2\,|t\right)=\Sigma_{LM}\,\Sigma_{l_1l_2}\,\frac{\Psi_{l_1l_2}^{(LM)}\left(r_1,r_2\,|t\right)}{r_1r_2}Y_{l_1l_2}^{L,M}\left(\Omega_1,\Omega_2\right),$$

for a specific symmetry (*LM*). After we expand the Coulomb repulsion term $1/\left|\mathbf{r}_1-\mathbf{r}_2\right|$ and the x-ray field interaction $\mathbf{E}_x(t)\square(\mathbf{r}_1+\mathbf{r}_2)$ in terms of spherical harmonics, substitute these expansions into the above Schrödinger Eq. (1), and integrate over the angles Ω_1 and Ω_2, we end up with a set of coupled partial differential equations with only two radial variables r_1 and r_2:

$$i\frac{\partial}{\partial t}\Psi_j\left(r_1,r_2\middle|t\right)=\left[\hat{T}_1+\hat{T}_2+\hat{V}_c\right]\Psi_j\left(r_1,r_2\middle|t\right)$$
$$+\sum_k\hat{V}_{j,k}^I\left(r_1,r_2\middle|t\right)\Psi_k\left(r_1,r_2\middle|t\right),$$

(2)

where each partial wave index j corresponds to a specific momentum combination (L, M, l_1, l_2). In Eq. (2), the diagonal operators $\hat{T}_1$, $\hat{T}_2$, and $\hat{V}_c$ give the kinetic energies and the Coulomb attractions between each electron and the nucleus, while the off-diagonal potential term $\hat{V}_{j,k}^I\left(r_1,r_2\middle|t\right)$ consists of the Coulomb interaction between two electrons and their interactions with external fields. Since the x-ray pulse is linearly polarized, we may set the magnetic quantum number to zero in the case of the singlet ($M = 0$) ground state chosen as the initial state.

Combining the real-space-product (RSP) algorithm with the finite-element discrete-variable representation (FEDVR) [33], we have developed a parallel code RSP–FEDVR–TDCC [34] accurately solving Eq. (2) on supercomputers for collisional and photionization problems [35–41]. For the calculations presented here, we have used up to 900 size-varied finite elements (FE's) with four-point DVR per FE, which gives a maximum radius of ~302 Bohr. Before the x-ray pulse interactions, we relaxed trial wave packets with 16 partial waves ($l_1 = l_2 = 0$ to 15 and $L = 0$) by the imaginary-time propagation and obtained ground-state energies for each of the cases. For the calculations presented here, we have used up to 900 size-varied finite elements (FE's) with four-point DVR per FE, which gives a maximum radius of ~302 Bohr. Before the x-ray pulse interactions, we relaxed trial wave packets with 16 partial waves ($l_1 = l_2 = 0$ to 15 and $L = 0$) by the imaginary-time propagation and obtained ground-state energies for each of the cases. The results are listed in Table I, in comparison with the values from National Institute of

Standards and Technology (NIST) [42], which shows an accuracy of $\Delta E/E < 0.05\%$ for all the cases. For the TPDI results presented here, we have used a total of 143 partial waves in our expansion with all possible combinations of angular momenta: $L = 0$ to 3 and $l_1 = l_2 = 0$ to 15. For the ground state ($L = 0$) absorbing two photons, the final outgoing two electrons have a well-defined total angular momentum of $L = 0, 2$ (S and D waves). Convergence has been reached with the parameters chosen.

TABLE I: The ground-state energies of He and He-like ions calculated by our (RSP–FEDVR–TDCC) code compared with the values reported by NIST.

Species	RSP–FEDVR–TDCC (atomic unit)	NIST (atomic unit)	$\Delta E/E$ (%)
He	−2.9033	−2.9034	0.003
Li$^+$	−7.2786	−7.2798	0.016
Be^{2+}	−13.6522	−13.6566	0.030
C^{4+}	−32.4008	−32.4160	0.047

III.   RESULTS AND DISCUSSIONS

We first consider TPDI of He and He-like ions with photon energies above the SPDI threshold to have the same excess energy of $E_{ex} \approx 50$ eV for each case. Namely, we have chosen x-ray pulses of $h\nu = \hbar\omega \approx 129$ eV, 248 eV, 421.4 eV, and 932 eV, respectively, for cases of He, Li$^+$, Be^{2+}, and C^{4+}. The linearly polarized x-ray pulses have intensities varying from $I = 5 \times 10^{16}$ W/cm^2 for He to $I = 10^{17}$ W/cm^2, 2×10^{17} W/cm^2, and 2×10^{18} W/cm^2 for Li$^+$, Be^{2+}, and C^{4+}, respectively. All the x-ray pulses had a pulse duration of $T_p = 500$ attoseconds with a sin^2

pulse shape, e.g. the x-ray pulse field is derived from $E(t) = -\partial A(t)/\partial t$ with the vector potential defined as $(t) = -(\frac{E_0}{\omega}) \times \sin^2[\frac{\pi(t+T_P/2)}{T_P}] \times \sin[\omega(t + \frac{T_P}{2})]$ and $-T_P/2 < t < T_P/2$.

After the pulse interaction, we further propagated the wave packet for another 500 attoseconds so that the outgoing TPDI electrons were far away (≥ 100 bohr) from the nucleus. The resulting electron probabilities at the end of simulation are shown by Fig. 1 on a plane spanned by the radial coordinates r_1 and r_2. For the chosen photon energies, the SPDI process resulted in the same excess energy so that the SPDI "ring" appears at the same location of $|r| \approx 68$ bohr in every panel. The two-photon double-ionization features show up at larger radii for Li^+, Be^{2+} to C^{4+}, as the larger photon energy boosts the TPDI electron wave packet to a higher momentum.
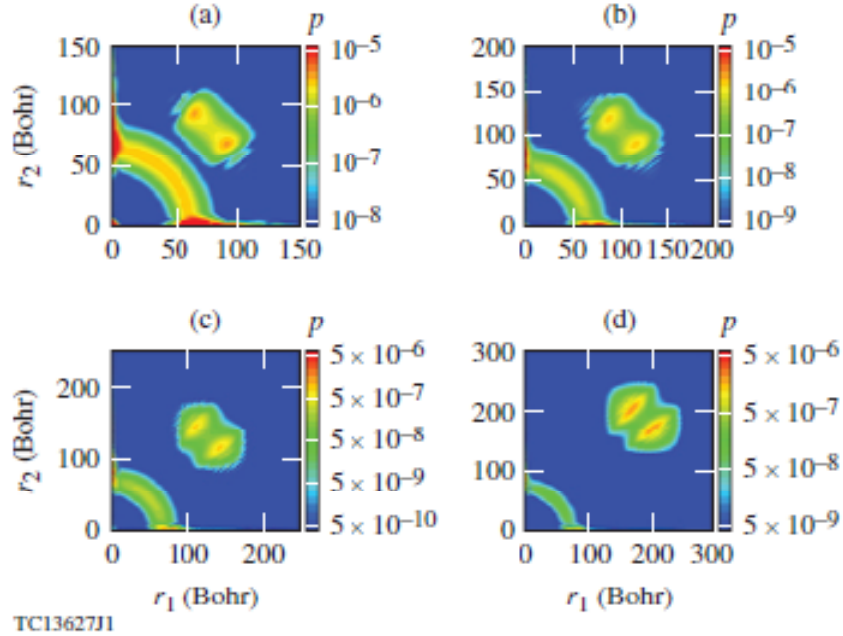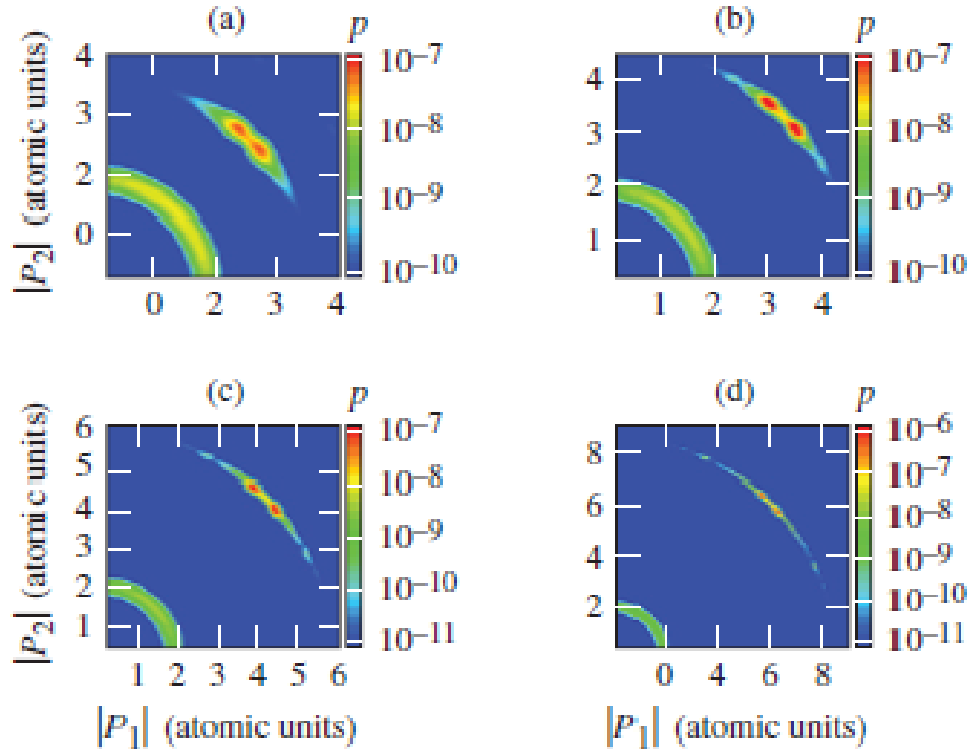

TC13627J1

FIG. 1. (Color online) The final photoionization probability–density distribution on the plane spanned by the radial coordinates r_1 and r_2, for (a) He and He-like ions of (b) Li^+, (c) Be^{2+}, and (d) C^{4+} exposed to intense x-ray pulses.

7

All four panels in Fig. 1 show two peaks in the TPDI probability distribution, which are close to what are expected from the sequential double-ionization path. Namely, if the two electrons independently absorb one photon each, we anticipate to finding one electron having an outgoing energy of $E_1 = h\nu - |Ip_1|$ and the other with $E_2 = h\nu - |Ip_2|$, where Ip_1 and Ip_2 are the ionization potentials of first and second electron, respectively, in these He isoelectron systems. Some interference features are also observed in the TPDI wave packets.

To see the momentum distribution of the outgoing electron wave packets, we projected the normalized double continuum $\left(\phi_{p_1 l_1} \text{ and } \phi_{p_2 l_2}\right)$ of corresponding ions onto the total wave function (after the ground state was projected out). The resulting ionizing-electron probability densities $\left[\Sigma_{L,l_1,l_2} \left|P_{l_1 l_2}^L (p_1, p_2)\right|^2\right]$ in momentum space are plotted in Fig. 2 for the four cases. Because of energy conservation, the outgoing electrons have maximum probabilities along two rings in the momentum space, corresponding to the SPDI and TPDI processes. Again, one sees that the SPDI ring appears at the same momentum of $|p| \approx 1.92$ a.u. (because of the same SPDI excess energy of $E_{\text{ex}} \approx 50$ eV). Now, Fig. 2 clearly shows the TPDI peaks at higher and higher "momentum rings" for the four cases varying from He in Fig. 2(a) to C^{4+} in Fig. 2(d). Also, we observe that the width of these momentum rings becomes narrower and narrower. This is due to the fact that for the same pulse duration (500 attoseconds) used, the bandwidth of the low-frequency ($h\nu = 129$ eV) x-ray pulse for the He case is much broader than the high-frequency ($h\nu = 932$ eV) x-ray pulse for the C^{4+} case in Fig. 2(d). It is also interesting to see that for He-like ions there are one or more additional weaker peaks on the TPDI momentum ring, besides the two dominant peaks; for example, Fig. 2(c) displays two additional momentum peaks at

$|p_1|/|p_2| \square$ 2.7/5.2 a.u. These additional peaks come from the "path" of single-photon single-ionization with core excitation in the TPDI process [26]. Namely, the He-isoelectron systems absorbing one photon can cause one electron ionization with the second electron being simultaneously promoted to excited states like $2p$ and $3p$ of residual He^+, Li^{2+}, Be^{3+}, C^{5+}; then the second photon will release these excited core electrons, leading to both electrons ending at the same TPDI momentum ring.

TC13628J1

FIG. 2. (Color online) The momentum distribution of photo-induced double ionization of (a) He and He-like ions of (b) Li^+, (c) Be^{2+}, and (d) C^{4+} exposed to intense x-ray pulses.

9

Now, we turn to the electron–electron correlations by calculating the triple-differential cross section (TDCS) of TPDI, which is defined as [26,28]

$$\frac{d^3\sigma}{dEd\Omega_1\Omega_2} = \frac{C}{p_1 p_2} \int dp_1 \int dp_2 \; \delta\!\left(\alpha - \tan^{-1}(p_2/p_1)\right)$$

$$\times \left| \sum_{L=0,2} \sum_{l_1 l_2} D_{l_1,l_2} P_{l_1 l_2}^{L}(p_1,p_2) Y_{l_1 l_2}^{L}(\Omega_1,\Omega_2) \right|^2 \tag{3}$$

with the hyper-spherical angle $\alpha = \tan^{-1}(p_2/p_1)$, the phase factor $D_{l_1,l_2} = (-i)^{l_1+l_2} e^{i(\sigma_{l_1}+\sigma_{l_2})}$

with the Coulomb phases σ_{l_1} and σ_{l_2}, and the constant $C = 4\omega^2 \big/ \left(I^2 \pi^2 T_p\right)$, which is related to

x-ray pulse parameters. The TDCS results for the corresponding cases are plotted in Fig. 3 as a

function of the second electron ejection angle (θ_2) and energy (E_2), given the first electron

being ejected along the x-ray pulse polarization direction ($\theta_1 = 0°$). Note that all TDCS results

presented in this paper are for the co-planar geometry, i.e., $\phi_1 = \phi_2 = 0°$. Figure 3 shows that the

back-to-back ejection ($\theta_1 = 0°$ and $\theta_2 = 180°$) has the largest probability, as expected. In Fig. 3,

the horizontal dashed lines mark the energies expected if independent STPDI occurs. One can

immediately find that for He the two peaks at $\theta_2 = 180°$ shift toward each other (i.e., away from

the expected STPDI energies), while the co-ejected two electrons ($\theta_2 = 0°$) repel each other

from STPDI. Note that the core-excitation path in TPDI is clearly visible in He-like ions (this

feature is hidden for He because of the broad bandwidth of x-ray pulse used). As discussed

above, the energy shifting away from STPDI manifests the energy sharing between the two

outgoing electrons in TPDI: the more-correlated electrons tend to more equally share the excess energy available for them.
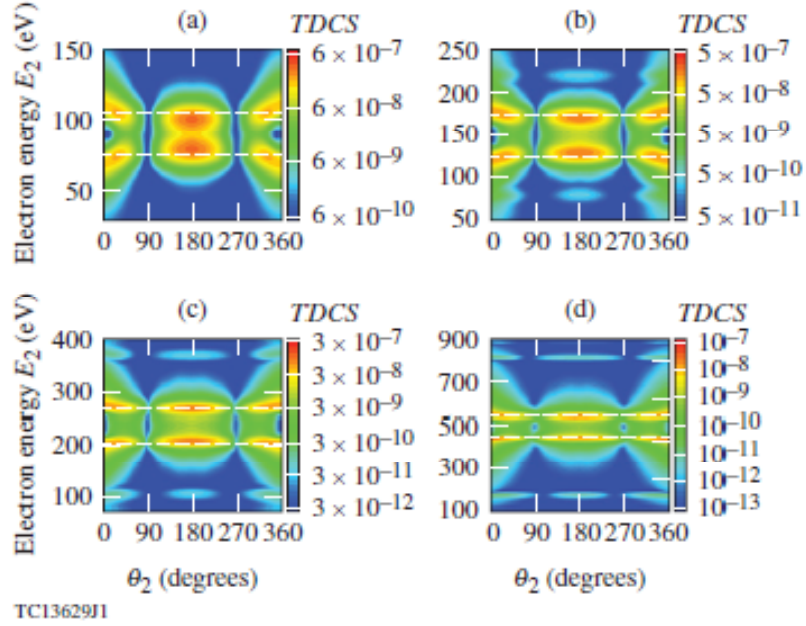

FIG. 3. (Color online) The triple-differential cross-section (TDCS) of two-photon double ionization (in units of 10^{-50} cm^4 s/sr^2 eV) as a function of the second electron ejection angle (θ_2) and energy (E_2) in the co-planar geometry ($\phi_1 = \phi_2 = 0°$), for the case of the first electron ejection angle of $\theta_1 = 0°$. The different panels correspond to the cases shown in Fig. 1, in which the horizontal dashed lines mark the expected energies from the sequential two-photon double ionization (STPDI).

Similar features are observed for the Li$^+$ and Be^{2+} cases in Figs. 3(b) and 3(c), although the energy shifts from STPDI get smaller and smaller. Finally, Fig. 3(d) shows a much smaller electron correlation for C^{4+}. Namely, the two electrons are ejected, almost following the

independent STPDI path. This is completely contrary to the intuition that the strongly correlated ground state and the stronger Coulomb field of C^{4+} should lead to more equal energy sharing between the two outgoing electrons.
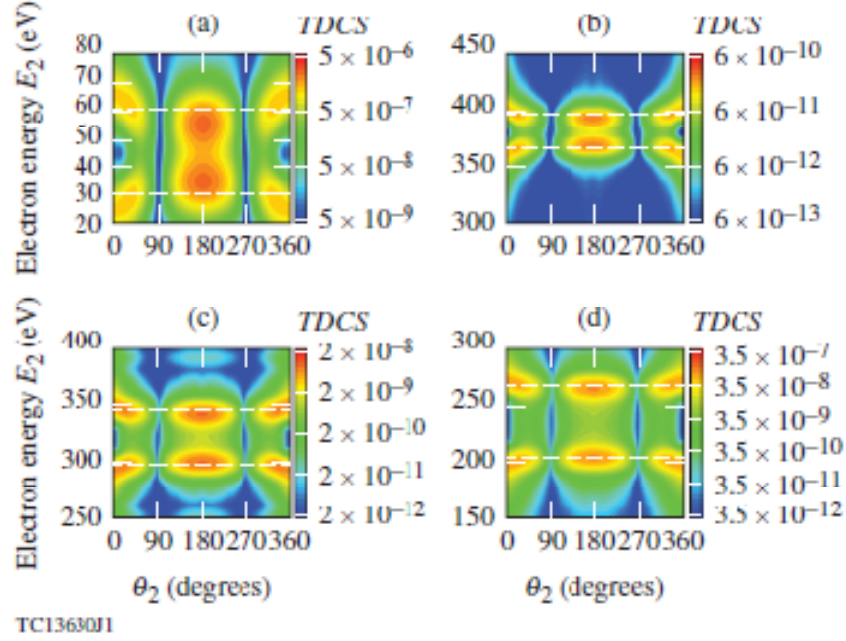

FIG. 4. (Color online) Similar to Fig. 3 but for He and He-like ions exposed to different x-ray pulses: (a) He with $h\nu = 85$ eV, (b) He with $h\nu = 421.4$ eV, (c) Li^+ with $h\nu = 421.4$ eV, and (d) Be^{2+} with $h\nu = 421.4$ eV, respectively. The same x-ray pulse intensity of $I = 2 \times 10^{17}$ W/cm^2 applies for (b)–(d), while $I = 5 \times 10^{16}$ W/cm^2 applies to (a).

To investigate if the observed electron correlation in TPDI of He-like ions is caused by the different photon energies chosen, we re-examined the three cases of He, Li^+, and Be^{2+} by using the same photon energy and intensity ($h\nu = 421.4$ eV and $I = 2 \times 10^{17}$ W/cm^2). The

12

resulting TDCS's are plotted in Figs. 4(b)–4(d) in the same energy scale. Again, one still sees more equal-energy sharing in He than in the Li$^+$ and Be^{2+} cases. In addition, Fig. 4(a) examines the case of He interacting with an x-ray pulse of hv = 85 eV and I = 5 × 10^{16} W/cm^2. In comparison with Figs. 3(a) and 4(b), Fig. 4(a) shows an even larger energy sharing (more away from STPDI). To understand the trend in TPDI energy sharing, we summarize these results in Fig. 5 by plotting the energy difference between the TPDI peak and the expected independent STPDI values for the different cases. Figure 5 unambiguously shows that the energy sharing of ~3 to 5 eV for He is a factor of ~5 larger than the C^{4+} case. We find that the overall feature of weaker electron correlation in TPDI of He-like ions is independent of x-ray photon energy and intensity.
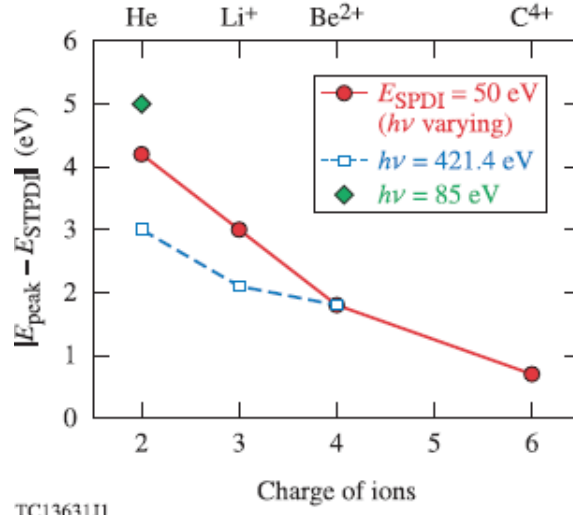

FIG. 5. (Color online) The energy shift of in the TPDI peak from the expected sequential TPDI locations as a function of Z of He-like ions, for the different cases investigated.

Note that for the main results presented in Figs. 3 and 5, we have kept the same excess energy ($E_{excess} = hv - |Ip_1| - |Ip_2| = 50\,eV$). Namely, these calculations are performed at

13

different kinematical regions. We wonder how the results may change if we compare the TPDI

process of He-like ions at the same kinematical condition. To explore this, we have fixed the

ratio of $E_{excess}/(|Ip_1|+|Ip_2|)$ to be ~7.6% for cases of He, Li$^+$ and Be^{2+} interacting with

different x-ray pulses: (a) $h\nu = 85$ eV and $I = 5\times 10^{16}$ W/cm^2 for He; (b) $h\nu = 213.1$ eV and $I =$

10^{17} W/cm^2 for Li$^+$; and (c) $h\nu = 399.7$ eV and $I = 2\times 10^{17}$ W/cm^2 for Be^{2+}. The resulting

triple-differential cross-sections (TDCS) of TPDI are plotted in Fig. 6 as a function of the ejected

electron energy of either electron-1 or electron-2 (*indistinguishable*), for these cases at the back-

to-back ejection geometry ($\theta_1 = 0°$ and $\theta_2 = 180°$). The vertical dashed lines mark the expected

locations if two electrons do not share the two-photon energy during ionization (i.e., the *STPDI*

path). Figure 6 shows the similar weakening electron correlation with increasing Z at the same

kinematical condition (peaks getting closer to the STPDI lines when nuclear charge increases).
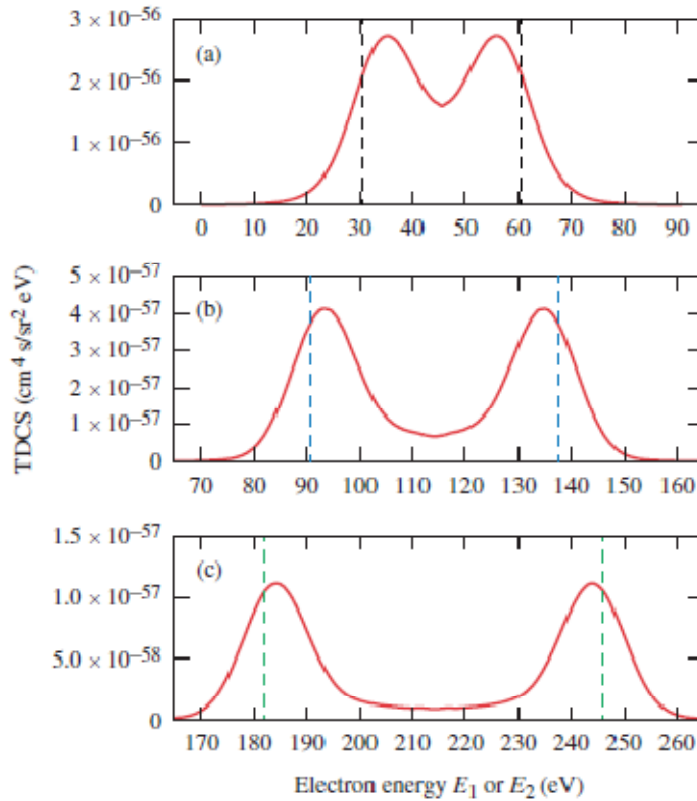

FIG. 6. (color online) TDCS *versus* the ejected electron energy for the back-to-back ejection geometry, for (a) He, (b) Li$^+$ and (c) Be^{2+} interacting with different x-ray pulses at the same ratio of $E_{excess}/(|Ip_1|+|Ip_2|) \approx 7.6\%$.

TC14044J1

14

These observations indicate that the final-state correlation determines the energy sharing in TPDI, instead of initial-state correlation. Namely, if each independent photon knocks out each individual electron into the continuum states, how long the two electrons keep interacting with each other in the continuum ultimately determines their energy sharing. The longer the two continuum electrons stay closer to each other, the more tendency they will exchange their energy efficiently. This "correlation time" should be inversely proportional to the relative velocity of the two electrons: $\delta v = \left| \sqrt{2(h\nu - |Ip_1|)} - \sqrt{2(h\nu - |Ip_2|)} \right|$. The larger their relative velocity, the quicker they come apart from each other, thereby being less correlated. Taking Fig. 3 as an example, this correlation time for He is the longest as the ionization potential difference between $|Ip_1|$ and $|Ip_2|$ is the smallest compared to other He-like ions [He ($Ip_1 \approx -24.59$ eV, $Ip_2 \approx -54.42$ eV) versus C^{4+} ($Ip_1 \approx -392.1$ eV, $Ip_2 \approx -490$ eV)]. Therefore, the two electrons from He tend to have more energy sharing than the He-like ions, thereby leading to more deviation from the STPDI picture. This argument also explains the more energy sharing for He and Li^+ with smaller photon energies (see Fig.5).

IV.   CONCLUSION

In summary, we have performed *ab initio* studies on the two-photon double ionization of He and He-like ions with x-ray pulses having photon energies above the SPDI threshold. We found that the electron correlation in TPDI of He-like ions becomes weaker and weaker as Z increases, which is opposite to the intuition that the strongly correlated ground state and the stronger Coulomb field of He-like ions might result in more correlated TPDI behavior. More investigations with different photon energies further confirm that the final-state correlation

determines the energy sharing between the two outgoing TPDI electrons. Namely, the more symmetric the velocity/energy of the two outgoing electrons, the longer the correlation time, thereby leading to more equal-energy sharing in the TPDI process of He than He-like ions. We hope that the new phenomenon and its physics insight revealed here can advance our understanding of the dynamic electron correlation in quantum systems.

References

1. R. Dörner, Th. Weber, M. Weckenbrock, A. Staudte, M. Hattass, H. Schmidt-Böcking, R. Moshammer, and J. Ullrich, Adv. At. Mol. Opt. Phys. **48**, 1 (2002).

2. J. Ullrich, R. Moshammer, A. Dorn, R. Dörner, L. Ph. H. Schmidt, and H. Schmidt-Böcking, Rep. Prog. Phys. **66**, 1463 (2003).

3. H. J. Wörner, J. B. Bertrand, B. Fabre, J. Higuet, H. Ruf, A. Dubrouil, S. Patchkovskii, M. Spanner, Y. Mairesse, V. Blanchet *et al.*, Science **334**, 208 (2011).

4. S. Sukiasyan, C. McDonald, C. Destefani, M. Yu. Ivanov, and T. Brabec, Phys. Rev. Lett. **102**, 223002 (2009).

5. T. Brabec and F. Krausz, Rev. Mod. Phys. **72**, 545 (2000).

6. W. Kohn and L. J. Sham, Phys. Rev. **140**, A1133 (1965).

7. W. Becker, X. Liu, P. Jo Ho, and J. H. Eberly, Rev. Mod. Phys. **84**, 1011 (2012).

8. I. Bray and A. T. Stelbovics, Phys. Rev. Lett. **70**, 746 (1993).

9. M. S. Pindzola and F. Robicheaux, Phys. Rev. A **57**, 318 (1998); **58**, 779 (E) (1998).

10. T. N. Rescigno, M. Baertschy, W. A. Isaacs, and C. W. McCurdy, Science **286**, 2474 (1999).

11. P. G. Burke and W. D. Robb, Adv. At. Mol. Phys. **11**, 143 (1976); M. A. Lysaght, P. G. Burke, and H. W. van der Hart, Phys. Rev. Lett. **102**, 193001 (2009).

12. R. Dörner, V. Mergel, O. Jagutzki, L. Spielberger, J. Ullrich, R. Moshammer, and H. Schmidt-Böcking, Phys. Rep. **330**, 95 (2000).

13. N. Berrah, F. Heiser, R. Wehlitz, J. Levin, S. B. Whitfield, J. Viefhaus, I. A. Sellin, and U. Becker, Phys. Rev. A **48**, R1733 (1993).

14. R. Dörner, J. M. Feagin, C. L. Cocke, H. Bräuning, O. Jagutzki, M. Jung, E. P. Kanter, H. Khemliche, S. Kravis, V. Mergel *et al.*, Phys. Rev. Lett. **77**, 1024 (1996); **78**, 2031(E) (1997).

15. A. S. Kheifets and I. Bray, Phys. Rev. A **58**, 4501 (1998); A. Knapp, A. Kheifets, I. Bray, Th. Weber, A. L. Landers, S. Schössler, J. Jahnke, J. Nickles, S. Kammer, O. Jagutzki *et al.*, Phys. Rev. Lett. **89**, 033004 (2002).

16. H. W. van der Hart, K. W. Kurt W. Meyer, and C. H. Chris H. Greene, Phys. Rev. A **57**, 3641 (1998).

17. B. Piraux, J. Bauer, S. Laulan, and H. Bachau, Eur. Phys. J. D **26**, 7 (2003).

18. L. Feng and H. W. van der Hart, J. Phys. B: At. Mol. Opt. Phys. **36**, L1 (2003).

19. A. Rudenko, L. Foucar, M. Kurka, Th. Ergler, K. U. Kühnel, Y. H. Jiang, A. Voitkiv, B. Najjari, A. Kheifets, S. Lüdemann *et al.*, Phys. Rev. Lett. 101, 073003 (2008); S. Askeland, R. Nepstad, and M. Førre, Phys. Rev. A **85**, 035404 (2012).

20. J. M. Ngoko Djiokap, N. L. Manakov, A. V. Meremianin, S. X. Hu, L. B Madsen, and A. F. Starace, Phys. Rev. Lett. **113**, 223002 (2014); C. Yu and L. B. Madsen, Phys. Rev. A **94**, 053424 (2016).

21. A. S. Kheifets and I. Bray, Phys. Rev. A **58**, 4501 (1998).

22. S. Otranto and C. R. Garibotti, Phys. Rev. A **67**, 064701 ((2003).

23. M Foster and J. Colgan, J. Phys. B: At. Mol. Opt. Phys. **39**, 5067 (2006).

24. T. Brabec, M. Yu. Ivanov, and P. B. Corkum, Phys. Rev. A **54**, R2551 (1996).

25. S. X. Hu and C. H. Keitel, Phys. Rev. A **63**, 053402 (2001).

26. J. Colgan and M. S. Pindzola, Phys. Rev. Lett. **88**, 173002 (2002).

27. A. Y. Istomin, N. L. Manakov, and A. F. Starace, J. Phys. B: At. Mol. Opt. Phys. **35**, L543 (2002).

28. S. X. Hu, J. Colgan, and L. A. Collins, J. Phys. B: At. Mol. Opt. Phys. **38**, L35 (2005).

29. S. X. Hu and L. A. Collins, Phys. Rev. Lett. **96**, 073004 (2006).

30. S. X. Hu and L. A. Collins, J. Mod. Opt. **54**, 943 (2007).

31. J. Feist, S. Nagele, R. Pazourek, E. Persson, B. I. Schneider, L. A. Collins, and J. Burgdörfer, Phys. Rev. A **77**, 043420 (2008).

32. M. S. Pindzola and F. Robicheaux, Phys. Rev. A **54**, 2142 (1996).

33. T. N. Rescigno and C. W. McCurdy, Phys. Rev. A **62**, 032706 (2000).

34. S. X. Hu, Phys. Rev. E **81** 056705 (2010); B. I. Schneider, L. A. Collins, and S. X. Hu, Phys. Rev. E **73**, 036708 (2006).

35. S. X. Hu and L. A. Collins, Phys. Rev. A **71**, 062707 (2005); S. X. Hu, Phys. Rev. A **74**, 062716 (2006).

36. S. X. Hu, Phys. Rev. Lett. **98**, 133201 (2007).

37. R.-F. Lu, P.-Y. Zhang, and K.-Li. Han, Phys. Rev. E **77**, 066701 (2008).

38. D. A. Horner, J. Colgan, F. Martin, C. W. McCurdy, M. S. Pindzola, and T. N. Rescigno, Phys. Rev. A **70**, 064701 (2004).

39. J. Feist, S. Nagele, C. Ticknor, B. I. Schneider, L. A. Collins, and J. Burgdörfer, Phys. Rev. Lett. **107**, 093005 (2011).

40. J. M. Ngoko Djiokap, S. X. Hu, W.-C. Jiang, L.-Y. Peng, and A. F. Starace, New J. Phys. **14**, 095010 (2012).

41. S. X. Hu, Phys. Rev. Lett. **111**, 123003 (2013).

42. NIST Atomic Spectra Database Lines Form, accessed 22 August 2017, https://physics.nist.gov/PhysRefData/ASD/lines_form.html.

Figure captions

FIG. 1. (Color online) The final photoionization probability–density distribution on the plane spanned by the radial coordinates r_1 and r_2, for (a) He and He-like ions of (b) Li^+, (c) Be^{2+}, and (d) C^{4+} exposed to intense x-ray pulses.

FIG. 2. (Color online) The momentum distribution of photo-induced double ionization of (a) He and He-like ions of (b) Li^+, (c) Be^{2+}, and (d) C^{4+} exposed to intense x-ray pulses.

FIG. 3. (Color online) The triple-differential cross-section (TDCS) of two-photon double ionization (in units of 10^{-50} cm^4 s/sr^2 eV) as a function of the second electron ejection angle (θ_2) and energy (E_2) in the co-planar geometry ($\phi_1 = \phi_2 = 0°$), for the case of the first electron ejection angle of $\theta_1 = 0°$. The different panels correspond to the cases shown in Fig. 1, in which the horizontal dashed lines mark the expected energies from the sequential two-photon double ionization (STPDI).

FIG. 4. (Color online) Similar to Fig. 3 but for He and He-like ions exposed to different x-ray pulses: (a) He with $h\nu = 85$ eV, (b) He with $h\nu = 421.4$ eV, (c) Li^+ with $h\nu = 421.4$ eV, and (d) Be^{2+} with $h\nu = 421.4$ eV, respectively. The same x-ray pulse intensity of $I = 2 \times 10^{17}$ W/cm^2 applies for (b)–(d), while $I = 5 \times 10^{16}$ W/cm^2 applies to (a).

FIG. 5. (Color online) The energy shift of in the TPDI peak from the expected sequential TPDI locations as a function of Z of He-like ions, for the different cases investigated.

FIG. 6. (color online) TDCS versus the ejected electron energy for the back-to-back ejection geometry, for (a) He, (b) Li^+ and (c) Be^{2+} interacting with different x-ray pulses at the same ratio of $E_{excess} / (|Ip_1| + |Ip_2|) \approx 7.6\%$.